The Astrophysical Journal Supplement Series, 146:467–477, 2003 June

ABSOLUTE PHOTOIONIZATION CROSS SECTION MEASUREMENTS OF O II IONS FROM 29.7 TO 46.2 eV

A. Aguilar, A. M. Covington, G. Hinojosa,[1] and R. A. Phaneuf
Physics Department, University of Nevada, Reno, NV 89557-0058

I. Álvarez and C. Cisneros
Centro de Ciencias Físicas, UNAM, Apartado Postal 6-96, Cuernavaca 62131, México

J. D. Bozek, I. Dominguez,[2] M. M. Sant'Anna,[3] and A. S. Schlachter
Advanced Light Source, Lawrence Berkeley National Laboratory, MS 7-200, Berkeley, CA 94720

S. N. Nahar
Department of Astronomy, Ohio State University, 174 West 18th Avenue, Columbus, OH 43210

and

B. M. McLaughlin[4]
ITAMP, Harvard Smithsonian Center for Astrophysics, 60 Garden Street, Cambridge, MA 02138
Received 2002 October 19; accepted 2002 December 12

ABSTRACT

Absolute photoionization cross sections have been measured for a mixture of ground-state and metastable O II (O^+) ions at photon energies ranging from 29.9 to 46.0 eV (414.7 to 269.5 Å). All measurements were performed by merging an O^+ beam with synchrotron radiation from an undulator beam line at the Advanced Light Source (ALS). At a resolution of 17 meV, more than 70 spectral features have been resolved, most of them identified and characterized. These measurements are compared with two independent *R*-matrix calculations and the data in TOPbase. All three calculations agree within 25% on the direct photoionization cross section, and with the absolute measurements within 40%. Some differences are noted in the predicted resonance positions among the three close-coupling *R*-matrix calculations, the TOPbase data being the least accurate. The estimated total experimental uncertainty varies from 15% to 20%. Such measurements benchmark theoretical photoionization cross section calculations performed within the framework of the Opacity Project and the Iron Project.

Subject headings: atomic data — atomic processes — methods: laboratory

1. INTRODUCTION

For decades absolute photoionization cross section calculations of positive ions have been performed using different approximations and techniques. In 1981 an international collaboration called the Opacity Project (OP) was formed to reestimate stellar envelope opacities in terms of atomic data computed by ab initio methods (Seaton 1987; Burke & Berrington 1993). This effort combined with the OPAL Project (Rogers & Iglesias 1992; Iglesias & Rogers 1996 and references therein) and the Iron Project (Hummer et. al. 1993), among others, have led to the creation of several atomic databases widely used for astrophysical calculations. For a description of these databases the reader is referred to a recent article (Mendoza 2000[5]). The OP atomic database (TOPbase) has been established at the Centre de Données Astronomiques de Strasbourg (CDS), France, for general access via the Internet (Cunto et al. 1993). Simultaneously, other independent calculations have been performed that include more atomic processes and basis states. However, these sets of atomic calculations have received little experimental verification, making it difficult, if not arbitrary, to resolve differences between them. The lack of experimental absolute photoionization cross sections can be attributed to the difficulty of producing a sufficiently high density of target ions and the required photon flux. These experimental difficulties have been overcome using merged ion-photon beams and synchrotron radiation. Employing this technique, the first absolute photoionization cross section measurement for a positive ion was obtained for Ba^+ in 1986 (Lyon et al. 1986). This was followed by the first group of absolute photoionization cross sections in Ca^+ (Lyon et al. 1987b), Sr^+ (Lyon, Peart, & Dolder 1987a), K^+ (Peart & Lyon 1987), and Ga^+ and Zn^+ (Peart, Lyon, & Dolder 1987). All these ions have in common large photoionization cross sections due to the $np \rightarrow nd$ autoionizing resonances but are of little significance for astrophysics. With the development of third-generation synchrotron radiation sources, a series of absolute photoionization cross section measurements for singly charged ions with greater astrophysical relevance was initiated in 1999 with K^+ (Kjeldsen et al. 1999a), C^+ (Kjeldsen et al. 1999b; Kjeldsen et al. 2001), Mg^+ (Kjeldsen et al. 2000b), I^+, I^{2+} (Kjeldsen et al. 2000a), and Fe^+ (Kjeldsen et al. 2002a). Moreover, absolute photoionization cross section measurements with unprecedented energy resolution have more recently become available for

[1] Present address: Centro de Ciencias Físicas, UNAM, Apartado Postal 6-96, Cuernavaca 62131, México.
[2] Present address: Centro Nacional de Metrología, CENAM, QRO 76241, México.
[3] Present address: Instituto de Física, Universidade Federal do Rio de Janeiro, Caixa Postal 68528, 21941-972 Rio de Janeiro RJ, Brazil.
[4] Present address: School of Mathematics and Physics, Queen's University, Belfast BT7 1NN, UK.
[5] Mendoza, C. 2000, Proc. Atomic Data Needs for X-Ray Astronomy, http://heasarc.gsfc.nasa.gov/docs/heasarc/atomic/, p. 167.

Ne^+ (Covington et al. 2002), challenging state-of-the-art methods for calculation of cross sections. Furthermore, recent combined studies on the doubly charged ions C^{2+} (Müller et al. 2002) and Sc^{2+} (Schippers et al. 2002) illustrate the importance of the symbiotic relationship between theory and experiment. For a summary of the advances in photoionization of atomic ions the reader is referred to a recent comprehensive review (West 2001).

Photoabsorption processes from low-lying metastable states of open-shell nitrogen-like ions are particularly important in astrophysical plasmas as well as in the upper atmosphere (Meier 1991). For instance, metastable states of O^+ are produced by photoionization in the F-region of the ionosphere (Carr, Niciejewski, & Killeen 1993; Melendez-Alvira et al. 1999). Three articles have special relevance to the present paper. Measurements of photoionization of metastable O^+ were recently reported (Covington et al. 2001). In that Letter, structure observed below the ground-state threshold was identified, but detailed information of about these features was not presented. Another important reference is the experiment performed at the ASTRID storage ring at the University of Århus on photoionization of N^+ and O^+ (Kjeldsen et al. 2002b). Resonance positions and oscillator strengths were reported for N^+ but not for O^+. The same group also measured absolute continuum cross sections and reported resonance positions and oscillator strengths for the homologous S^+ system (Kristensen et al. 2002). In the present paper, the identification and characterization of most of the 45 features observed from the $^2P^o$ metastable-state threshold at 30.104 eV to the $^4S^o$ ground-state threshold at 35.121 eV are summarized in a table. Furthermore, the energy range is extended to 46.0 eV, and 30 additional features are resolved, identified, and characterized. All reported measurements were taken at a photon energy resolution of 17 meV, which compares to 30–150 meV for the data of the Århus group.

2. EXPERIMENT

Absolute cross section measurements for photoionization of a mixture of ground state and metastable states of O^+ at photon energies ranging from 29.9 to 46.0 eV (414.7 to 269.5 Å) were performed at the Ion-Photon-Beam (IPB) end station installed at undulator beam line 10.0.1 of the Advanced Light Source (ALS) at Lawrence Berkeley National Laboratory. A schematic drawing of the IPB end station is shown in Figure 1. The main features of the apparatus and the technique used to determine the metastable fractions of O^+ are described here. Further details may be found elsewhere (Covington et al. 2002). The oxygen ions were produced by injecting CO gas into a hot-filament low-pressure discharge ion source. The accelerated ions (6 keV) are directed and selected according to their mass per charge ratio by a 60° analyzing magnet. The O^+ beam was merged onto the axis of the photon beam by a 90° spherical electrostatic deflector. The interaction region consists of a 29.4 cm long cylindrical mesh tube located in the interaction path that was biased at +2 kV. The O^{2+} product ions produced inside the interaction region were thereby labeled with a kinetic energy of 8 keV in the downstream region. The two-dimensional spatial profiles of the merged ion and photon beams are monitored using commercial rotating-wire beam-profile monitors located just upstream and downstream of the interaction region, and a translating-slit scanner at the midpoint. A second analyzing magnet and spherical electrostatic deflecting plates are used to separate and deflect out of the plane of dispersion the O^{2+} products produced in the interaction region from the primary beam and from O^{2+} ions produced elsewhere in the merged path. Ultrahigh vacuum conditions minimized the O^{2+} background produced by stripping collisions of O^+ with residual gas. This background was subtracted by mechanically chopping the photon beam. The product ions are guided to a negatively biased stainless steel plate from which secondary electrons are accelerated and impact a microsphere plate (MSP) detector. The primary ion beam (O^+) was collected and continuously monitored in a Faraday cup. The absolute detection efficiency (0.211 ± 0.011) was determined by measuring the O^{2+} current using a high-sensitivity subfemtoammeter and comparing it to the observed count rate.

All measurements were carried out at the 10 cm–period undulator beam line 10.0.1 at the Advanced Light Source

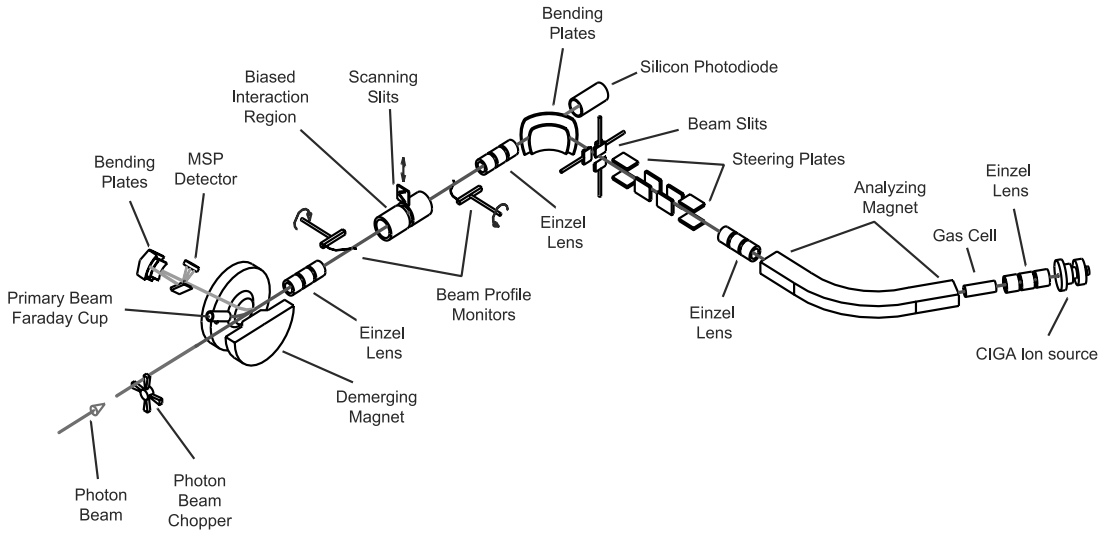

FIG. 1.—Ion-Photon-Beam (IPB) end station installed at ALS beam line 10.0.1

TABLE 1
TYPICAL EXPERIMENTAL PARAMETERS FOR ABSOLUTE PHOTOIONIZATION CROSS SECTION MEASUREMENTS AT A PHOTON ENERGY OF 33.0 eV

Parameter	Value
Ion beam energy (kV)	6
Interaction region bias (kV)	+2
O^{2+} signal rate (s^{-1})	285
Beam overlap factors (cm^{-2})	22.6, 16.1, 20.1
Merged path length (cm)	29.4
Ion collection efficiency	1.0 +0, −0.02
Photoion detection efficiency	0.211 ± 0.011
Ion beam current (nA)	68
Photon flux (photons s^{-1})	4.69×10^{13}
Ion velocity (O^+) (m s^{-1})	2.69×10^5
O^{2+} background rate (s^{-1})	107
Photodiode quantum yield (e photon^{-1})	9.5
Pulse transmission constant (%)	73.7
Cross section (Mb)	3.22 ± 0.17

(ALS) with a grazing incidence monochromator fitted with a 380 lines mm^{-1} grating. This beam line provides a photon flux of about 5×10^{13} photons s^{-1} at a resolving power of 2000 in the energy range of the present measurements. The photon flux was monitored using a calibrated Si *p-n* junction photodiode. The photon energy scale was calibrated using known ionization thresholds (from the NIST Atomic Spectra Database[6]) for ground-state and metastable O^+, with an uncertainty estimated to be ±5 meV. Typical parameters of the experiment are presented in Table 1.

2.1. *Determination of Metastable Fractions*

It is known that in hot-filament type discharge ion sources, ions are produced in metastable states as well as the ground state. There are two low-lying metastable states of O^+, $^2P^o$ and $^2D^o$, with mean lifetimes of 14 s and 1.3 hr, respectively (Wiese, Fuhr, & Deters 1996). In order to obtain the ground state fraction of the ion beam, an auxiliary experiment was performed in situ based on charge transfer measurements. The technique is based on the beam attenuation method described by Lindsay et al. (1998). It consists of passing all the ions extracted from the source through a gas cell containing N_2 before the analyzing magnet (see Fig. 1). The metastable components of the O^+ beam undergo a near-resonant charge exchange process with the nitrogen molecules and are preferentially neutralized. Figure 2 presents a plot of the transmitted O^+ beam current as a function of N_2 pressure in the gas cell (dots) measured with a wide-range ionization gauge. A 4 keV O^+ beam energy was used for this measurement, since the difference in the O^+–N_2 charge transfer cross sections between the ground state and metastable states increases as the O^+ beam energy decreases (see Fig. 5 in Lindsay et al. 1998). However, the cross sections for charge transfer with N_2 for the $^2P^o$ and $^2D^o$ metastable ions in O^+ ion beams are not sufficiently different to be distinguishable by the attenuation method. To determine the ground-state fraction, a sum of

[6] Martin, W. C., et al. 2002, NIST Atomic Spectra Database. Available at http://physics.nist.gov/asd (version 2.0) National Institute of Standards and Technology, Gaithersburg, MD.

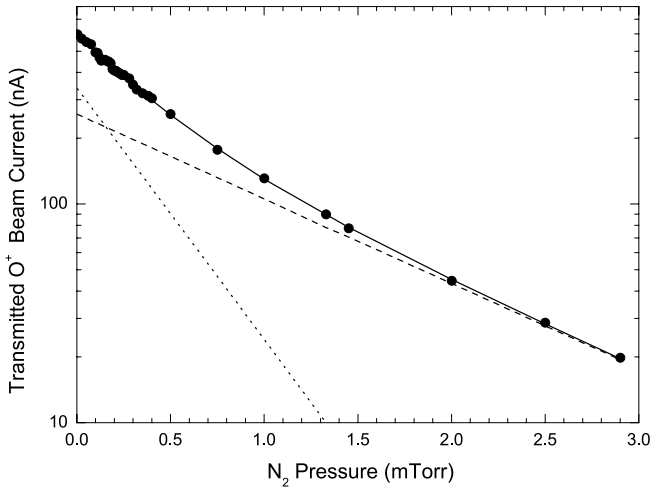

FIG. 2.—Ion beam attenuation measurements as a function of N_2 pressure. The dots are experimental measurements, and the solid line is a fit of the sum of two exponential functions to these data, represented by the dashed and dotted lines. The ratio of cross sections for the metastable and ground state components obtained from the fit is consistent with previous measurements (Lindsay et al. 1998).

two exponential functions (eq. [1]) was fitted to the experimental data (Fig. 2, *solid line*):

$$I = I_1 e^{-nl\sigma_1} + I_2 e^{-nl\sigma_2} , \quad (1)$$

where I_1 and I_2 are the initial intensities of the components of the beam and σ_1 and σ_2 are their cross sections for removal from the beam. The presence of two components is evidenced by the quality of the fit to the data. From this measurement, it was determined that the O^+ beam used for the photoionization measurements was composed of 43% ground state ($^4S^o$) and 57% metastable states ($^2P^o$ and $^2D^o$). In order to estimate the $^2P^o$ and $^2D^o$ fractions, it was assumed that the theories correctly predict the direct photoionization cross section for the $^2P^o$ metastable state at 31.15 eV. The corresponding fractions of 15% $^2P^o$ and 42% $^2D^o$ were obtained.

3. THEORY

The theoretical calculations were performed using the *R*-matrix method (Seaton 1987; Burke & Berrington 1993). In the close-coupling approximation the core ion is represented by an *N*-electron system, and the total wavefunction expansion, $\Psi(E)$, of the $(N + 1)$ electron system for any symmetry $SL\pi$ is expressed as

$$\Psi(E) = A \sum_i \chi_i \theta_i + \sum_j c_j \Phi_j , \quad (2)$$

where A is the antisymmetrization operator, χ_i is the core wavefunction in a specific state $S_i L_i \pi_i$, and θ_i is the wavefunction for the $(N + 1)$th electron in a channel labeled as $S_i L_i \pi_i k_i^2 \ell_i (SL\pi)$; k_i^2 being its incident kinetic energy. The Φ_j values are the correlation functions of the $(N + 1)$-electron system that account for short-range correlation and the orthogonality between the continuum and the bound orbitals. $\Psi(E)$ is a bound $(N + 1)$-electron wavefunction when the energy $E < 0$ with all channels closed, and a free or

continuum wavefunction when $E > 0$ with some or all continuum channels open.

3.1. *Theory A*

In the first *R*-matrix calculation (A), cross sections for the three terms of the O^+ electronic configuration, $2s^22p^3(^4S^o, ^2D^o, ^2P^o)$, were obtained from the close-coupling approximation. Multiconfiguration expansions were employed for the 12 core O^{2+} states, including orbitals up to 3*s*, with configurations of the form $2s^22p^2$, $2s2p^3$, $2s^22p3s$, and $2p^4$ (Nahar 1998). The 3*p*, 3*d*, 4*s*, and 4*p* orbitals used were correlated, allowing one to represent states, such as $2s^22p3s(^3P^o)$, which are important in photoionization because they correspond to strong dipole-allowed transitions in the core, and enhance the background cross sections. All possible channels with the free electron angular momentum, $l \leq 9$, are considered, which generates all prominent resonances in the respective cross sections via channel couplings.

3.2. *Theory B*

In the second *R*-matrix calculation (B), 26 states of the O^{2+} product ion were initially retained in the close-coupling calculations for the $^4S^o$ ground state and the $^2D^o$ and $^2P^o$ metastable states where orbitals were included only up to the 4*d* (Aggarwal & Hibbert 1991a). For this open shell ion, electron correlation is difficult to represent adequately with this restricted $n = 4$ basis. The limitations are apparent when compared to experiment (Covington et al. 2001), particularly in the energy range 35–40 eV, for the initial $O^+(^2P^o)$ and $O^+(^2D^o)$ metastable states, even with triple promotions in the scattering wavefunctions. A more elaborate and compact $n = 5$ basis (Aggarwal & Hibbert 1991b) was utilized to yield a truer representation of the experimental data, for both the $^4S^o$ ground state and the $^2D^o$, $^2P^o$ metastable states over the entire experimental energy range studied, from the $O^+(^2P^o)$ threshold to 46.0 eV. Here again, all of the 26 O^{2+} states were represented by multiconfiguration interaction wavefunctions, and the *R*-matrix calculations were performed with 20 continuum functions and a boundary radius of 10.0 Bohr radii. The O^+ photoionization cross section calculations were performed in *LS* coupling with the scattering wavefunctions generated by allowing all possible two-electron promotions out of the base $2s^22p^3$ configuration of O^+ into the orbital set employed. Using this extended $n = 5$ basis of Aggarwal & Hibbert (1991b) the outer region scattering problem was solved using a fine energy mesh of 0.136 meV between thresholds. This energy mesh was necessary in order to fully resolve the resonance structure in the respective photoionization cross sections when convoluted at the appropriate experimental spectral resolution of 17 meV. Experimentally it is extremely difficult to produce a beam of ground state O^+ ions without contamination from metastable states. Hence, in order to compare with experiment the theoretical cross sections for each initial state were weighted with the appropriate experimental fractions (0.15 $[^2P^o]$, 0.42 $[^2D^o]$ and 0.43 $[^4S^o]$, respectively) and summed.

TABLE 2

UNCERTAINTIES IN ABSOLUTE CROSS SECTION MEASUREMENTS ESTIMATED AT 90% CONFIDENCE LEVEL

Source	Relative (%)	Absolute (%)	Total (%)
Counting statistics	3	...	3
Photoion detector efficiency	...	5	5
Photoion collection efficiency	2	2	3
Pulse counting efficiency	...	3	3
Primary ion collection efficiency	...	2	2
Ion current measurement	...	2	2
Photodiode responsivity	3	6	7
Photodiode current measurement	2	2	3
Beam profile measurement	3	7	8
Beam overlap integral	10	7	12
Interaction length	...	2	2
Quadrature sum	12	14	18

4. RESULTS

Absolute cross section measurements reported for photoionization of the metastable states ($^2P^o$ and $^2D^o$) of O^+ ions from 29.8 to 35.5 eV (Covington et al. 2001) have been extended beyond the ground-state ($^4S^o$) threshold at 35.121 to 46.2 eV. The previous measurements are included to broaden the description of the O^+ *L*-shell photoionization spectrum. The data for a mixture of metastable and ground state O^+ ions are presented over the whole energy range in Figures 3, 4, 5, 6, and 7. The measured photoion yield spectrum has been normalized to absolute photoionization cross section measurements shown as open circles in Figures 3–7, with error bars estimated at 90% confidence level. Just above the ground-state threshold, the normalization presented here differs slightly from that reported previously (Covington et al. 2001). The sources of uncertainty and their estimated magnitudes are listed in Table 2. Table 3 compares the present absolute measurements taken at four energies above the ground-state threshold with theoretical predictions (weighted by the measured initial state

TABLE 3

COMPARISON OF ABSOLUTE MEASUREMENTS ABOVE THE GROUND STATE THRESHOLD WITH MEASUREMENTS OF KJELDSEN ET AL. 2002b AND THEORY

Energy (eV)	Present[a] (Mb)	Kjeldsen et al. (Mb)	TOPbase (Mb)	Theory A (Mb)	Theory B (Mb)
36.0	10.6 (1.6)	8.4	8.9	8.8	8.5
39.1	11.2 (2.7)	7.2	8.6	7.7	6.9
41.1	10.6 (2.2)	7.3	7.0	7.6	7.2
44.4	9.8 (1.7)	6.8	7.4	7.2	7.0

[a] Total uncertainty in parentheses.

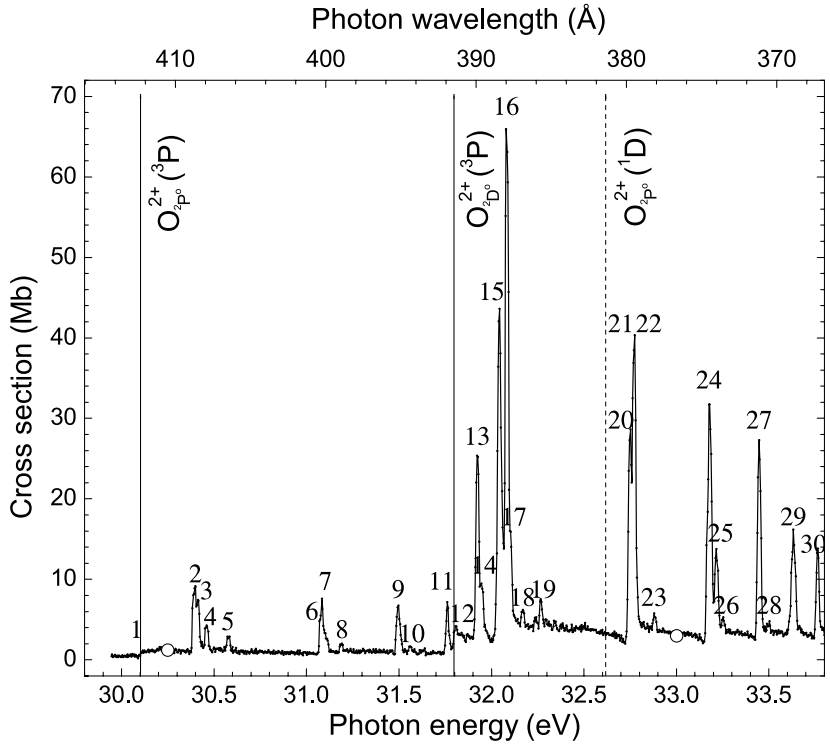

FIG. 3.—Photoionization cross section measurements for O^+. The two solid vertical lines show the ^3P photoionization threshold for the metastable states $^2P^o$ and $^2D^o$ of O^+, respectively. The vertical dashed line indicates the ^1D excited state of O^{2+}, which is the series limit of three Rydberg series $2s^22p^2$ (^1D)*nd* (^2P, ^2S) and *ns* (^2D) from the $^2P^o$ metastable state. The open circles are absolute cross section measurements to which the photoion yield spectrum has been normalized.

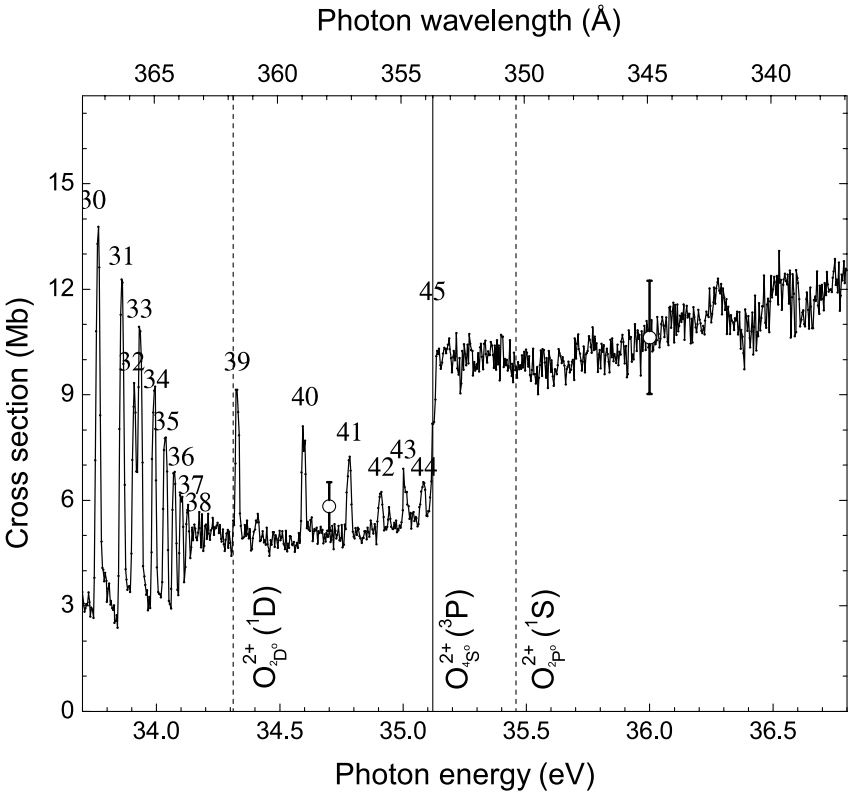

FIG. 4.—Photoionization cross section measurements for O^+. The solid vertical line shows the ^3P photoionization threshold for the ground state $^4S^o$ of O^+. The two vertical dashed lines indicate the ^1D and ^1S excited states of O^{2+}, respectively. The ^1D state is the series limit of four Rydberg series $2s^22p^2$ (^1D)*nd* (^2F, ^2D, ^2P), and *ns*(^2D) from the $^2D^o$ metastable state. The open circles are absolute cross section measurements to which the spectrum has been normalized.

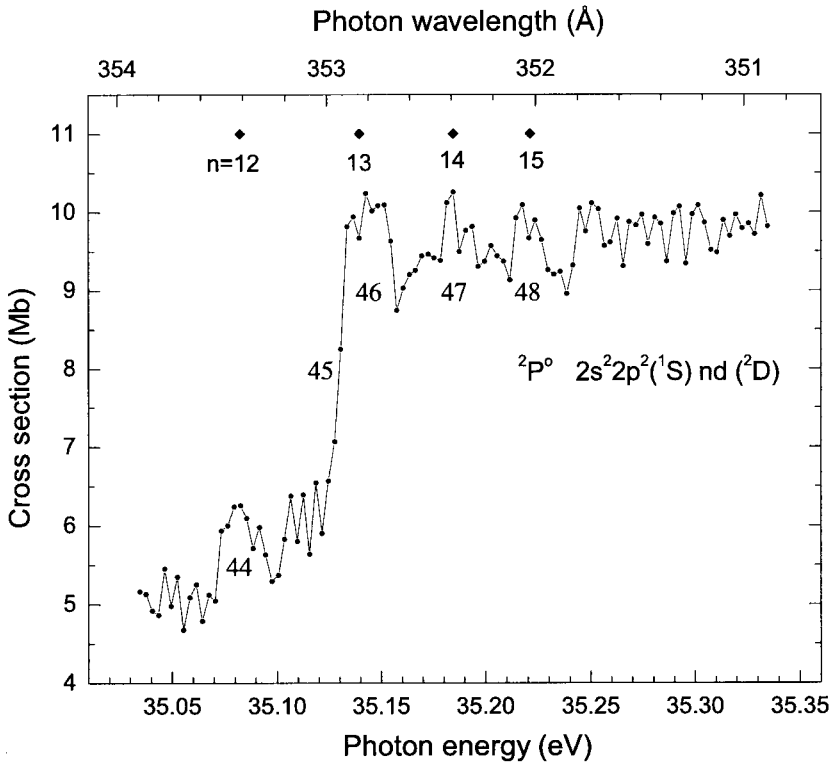

FIG. 5.—Magnified view of the ^3P photoionization threshold from the ground state $^4S^o$ of O^+. Members $n = 12$ to $n = 15$ of the $2s^22p^2(^1S)nd(^2D)$ Rydberg series from the $^2P^o$ metastable state are evident.

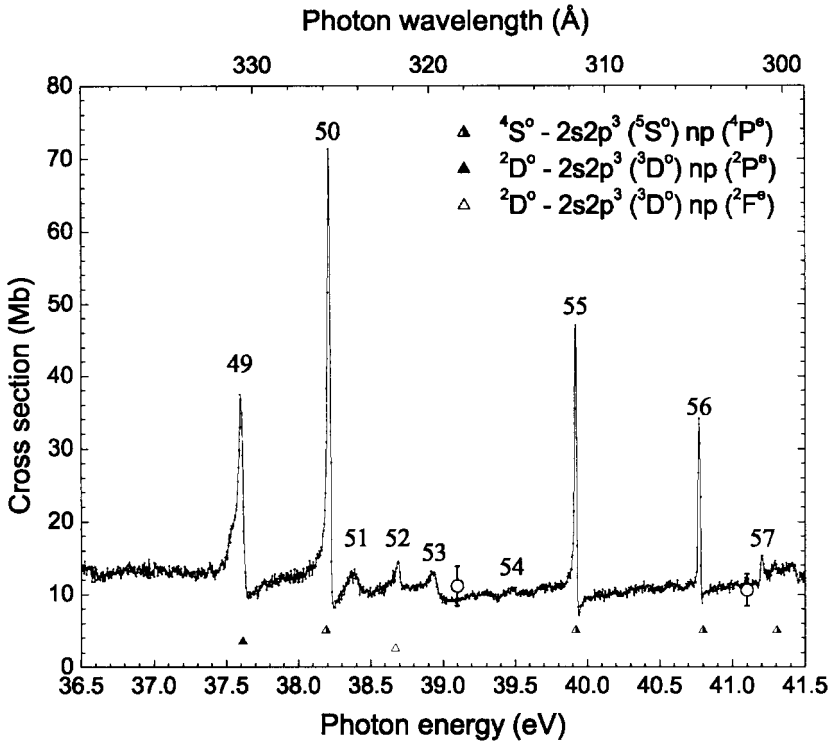

FIG. 6.—Photoionization cross section measurements for O^+. The beginnings of three Rydberg series are shown. The half-full triangles indicate the only Rydberg series observed from the ground state. The solid and open triangles show the positions of the members of the two Rydberg series from the $^2D^o$ metastable state. The open circles are absolute cross section measurements to which the spectrum has been normalized.

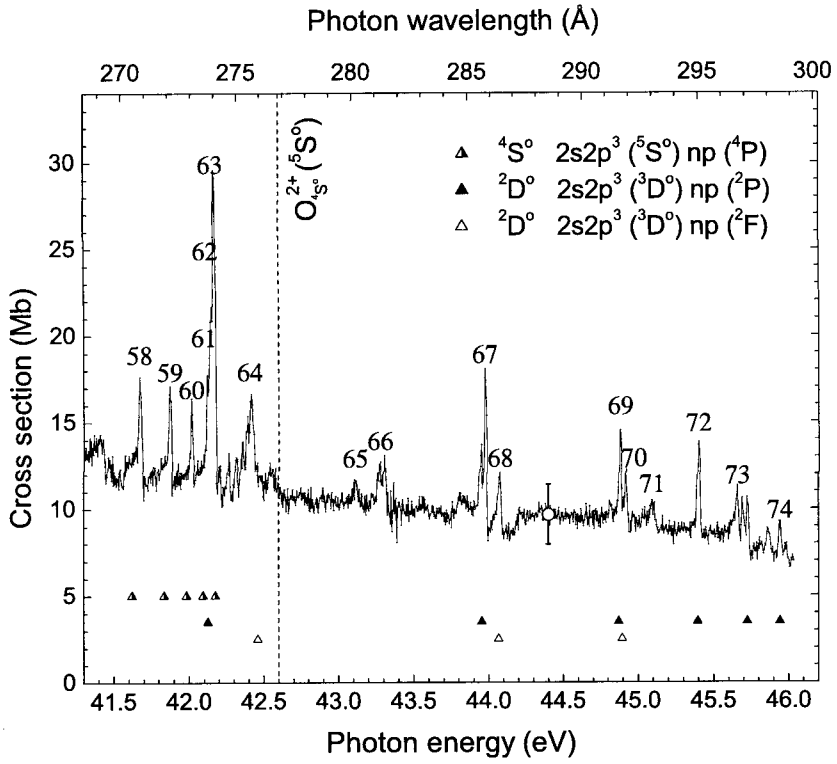

FIG. 7.—Photoionization cross section measurements for O^+. The vertical dashed line indicates the $^5S^o$ excited state of O^{2+}, which is the limit for the series $2s2p^3(^5S^o)np(^4P)$ from the $^4S^o$ ground state.

fractions) and the measurements of the Århus group (Kjeldsen et al. 2002b). This comparison is not strongly dependent on the metastable fractions, since the nonresonant cross sections are predicted by theory to be nearly the same for the ground state and metastable states.

All 45 features shown in Figures 3 and 4, with the exception of resonance number 3, were identified as members of six different Rydberg series (Covington et al. 2001). The common ^3P ionization limit for the ground state and metastable states of O^+ is clearly indicated by the steps in the data identified by numbers 1, 12, and 45 and marked with solid vertical lines on Figures 3 and 4. These steps correspond to the thresholds for direct photoionization from the $^2P^o$ metastable state at 30.104 eV, from the $^2D^o$ metastable state at 31.800 eV and from the $^4S^o$ ground state at 35.121 eV, respectively. The latter is shown on an expanded energy scale in Figure 5. All resonances below the $^4S^o$ threshold are due to the excitation of a $2p$ valence electron ($2p \rightarrow ns$ or $2p \rightarrow nd$) of either the $^2D^o$ or $^2P^o$ metastable states of O^+ to an excited state embedded in the continuum $^3P^e + ke^-$. In this energy range, four Rydberg series are observed from the $^2P^o$ metastable state: $2p^2(^1D)nd\ ^2P$, $2p^2(^1D)nd\ ^2S$, $2p^2(^1D)ns\ ^2D$, and $2p^2(^1S)nd\ ^2D$. From the $^2D^o$ metastable state four Rydberg series are also identified, $2p^2(^1D)nd\ ^2F$, ^2D, ^2P, and $2p^2(^1D)ns\ ^2D$. Note that the Rydberg states $2p^2(^1D)nd\ ^2P$ and $2p^2(^1D)ns\ ^2D$ are reached from both metastable states, giving rise to four distinct Rydberg series.

Above the $^4S^o$ ionization threshold the situation is different. The strong coupling between the ejection of the $2p$ and $2s$ valence electrons leads to asymmetric resonance line shapes (see Figs. 6 and 7). This effect has been previously studied theoretically for the photoionization of the $^4S^o$ ground state of atomic nitrogen (Le Dourneuf, Vo Ky Lan, & Zeippen 1979). In this energy range a single Rydberg series is observed originating from the $^4S^o$ ground state. This series starts at feature 50 followed by 55–59, 61, and 63. The reason for the anomalous intensity of feature 57 is unclear. It is possible to distinguish the first three members of this series in the experimental data reported previously by the Århus group (Kjeldsen et al. 2002b). Two additional Rydberg series are observed in the present experiment in this energy range. These series, which originate from the $^2D^o$ metastable state, are identified as $2s2p^3(^3D^o)np\ ^2P$ and ^2F. The first series is the strongest of the two, starting at feature number 49 and leaving little doubt about its assignment. The second is much weaker, and its assignment is uncertain. Three more features (54, 66, and 73) are observed close to the energies expected for the series $2s2p^3(^3P^o)nd\ ^2D$ from the $^2P^o$ metastable state. However, these assignments are much less certain. Table 4 presents the energy, quantum defect, oscillator strength, series limit, and assignment of each numbered feature in Figures 3–7. The oscillator strengths have been obtained by fitting a Gaussian to the majority of the features. In those cases where the line shape is strongly asymmetric, a Fano-Voigt profile was used.

All resonance assignments are based on quantum-defect theory and were simplified because the first members of most of the Rydberg series have been previously observed as absorption lines and their energies are reported in the NIST database (see footnote 6). To our knowledge none of the resonant energies in Table 4 have been previously reported, with the exception of those corresponding to excitation from $^2P^o$, $^2D^o$ to $2s^22p^2(^2D)6s\ ^2D$, indicated by feature numbers 5 and 19, respectively. The resonances associated with the metastable states below the ^4S threshold have been previously assigned (Covington et al. 2001; Kjeldsen et al. 2002b).

TABLE 4

FEATURE NUMBERS, ENERGIES, QUANTUM DEFECTS, OSCILLATOR STRENGTHS, SERIES LIMITS, AND ASSIGNMENTS

Feature	Energy (eV)	Quantum Defect δ	Oscillator Strength[a]	Series Limit (eV)	Assignment
1	30.104	...	...	...	$^2P^o$ threshold
2	30.393	0.054	0.0095	32.617	$^2P^o$–$2s^22p^2(^1D)5d(^2P)$
3	30.413	0.031	0.0086	32.617	$^2P^o$–$2s^22p^2(^1D)5d(^2S)$
4	30.460	...	0.0023	...	Unassigned
5	30.578	0.834	0.0023	32.617	$^2P^o$–$2s^22p^2(^1D)6s(^2D)$
6	31.081	0.048	0.0073	32.617	$^2P^o$–$2s^22p^2(^1D)6d(^2P)$
7	31.105	0.001	0.0030	32.617	$^2P^o$–$2s^22p^2(^1D)6d(^2S)$
8	31.188	0.829	0.0009	32.617	$^2P^o$–$2s^22p^2(^1D)7s(^2D)$
9	31.496	0.033	(0.0079)	32.617	$^2P^o$–$2s^22p^2(^1D)7d(^2P)$
	...	0.033	...	32.617	$^2P^o$–$2s^22p^2(^1D)7d(^2S)$
10	31.561	0.822	0.0007	32.617	$^2P^o$–$2s^22p^2(^1D)8s(^2D)$
11	31.762	0.023	(0.0058)	32.617	$^2P^o$–$2s^22p^2(^1D)8d(^2P)$
	...	0.023	...	32.617	$^2P^o$–$2s^22p^2(^1D)8d(^2S)$
12	31.800	...	...	...	$^2D^o$ threshold
13	31.924	0.076	0.0269	35.458	$^2P^o$–$2s^22p^2(^1S)4d(^2D)$
14	31.948	−0.017	(0.0090)	32.617	$^2P^o$–$2s^22p^2(^1D)9d(^2P)$
	...	−0.017	...	32.617	$^2P^o$–$2s^22p^2(^1D)9d(^2S)$
15	32.044	0.097	0.0253	34.311	$^2D^o$–$2s^22p^2(^1D)5d(^2F)$
16	32.083	0.054	[0.0352][b]	34.311	$^2D^o$–$2s^22p^2(^1D)5d(^2D)$
	...	−0.092	...	32.617	$^2P^o$–$2s^22p^2(^1D)10d(^2P)$
	...	−0.092	...	32.617	$^2P^o$–$2s^22p^2(^1D)10d(^2S)$
17	32.107	0.028	0.0024	34.311	$^2D^o$–$2s^22p^2(^1D)5d(^2P)$
18	32.169	−0.018	(0.0024)	32.617	$^2P^o$–$2s^22p^2(^1D)11d(^2P)$
	...	−0.018	...	32.617	$^2P^o$–$2s^22p^2(^1D)11d(^2S)$
19	32.267	0.836	0.0028	34.311	$^2D^o$–$2s^22p^2(^1D)6s(^2D)$
20	32.753	0.084	0.0061[c]	34.311	$^2D^o$–$2s^22p^2(^1D)6d(^2F)$
21	32.775	0.042	0.0100[c]	34.311	$^2D^o$–$2s^22p^2(^1D)6d(^2D)$
22	32.786	0.021	0.0014[c]	34.311	$^2D^o$–$2s^22p^2(^1D)6d(^2P)$
23	32.881	0.825	0.0010	34.311	$^2D^o$–$2s^22p^2(^1D)7s(^2D)$
24	33.179	0.057	(0.0172)	34.311	$^2D^o$–$2s^22p^2(^1D)7d(^2F)$
	...	0.057	...	34.311	$^2D^o$–$2s^22p^2(^1D)7d(^2D)$
	...	0.057	...	34.311	$^2D^o$–$2s^22p^2(^1D)7d(^2P)$
25	33.217	0.072	0.0157	35.458	$^2P^o$–$2s^22p^2(^1S)5d(^2D)$
26	33.251	0.825	0.0005	34.311	$^2D^o$–$2s^22p^2(^1D)8s(^2D)$
27	33.448	0.046	(0.0114)	34.311	$^2D^o$–$2s^22p^2(^1D)8d(^2F)$
	...	0.046	...	34.311	$^2D^o$–$2s^22p^2(^1D)8d(^2D)$
	...	0.046	...	34.311	$^2D^o$–$2s^22p^2(^1D)8d(^2P)$
28	33.498	0.804	0.0003	34.311	$^2D^o$–$2s^22p^2(^1D)9s(^2D)$
29	33.632	0.028	(0.0072)	34.311	$^2D^o$–$2s^22p^2(^1D)9d(^2F)$
	...	0.028	...	34.311	$^2D^o$–$2s^22p^2(^1D)9d(^2D)$
	...	0.028	...	34.311	$^2D^o$–$2s^22p^2(^1D)9d(^2P)$
30	33.763	−0.008	(0.0049)	34.311	$^2D^o$–$2s^22p^2(^1D)10d(^2F)$
	...	−0.008	...	34.311	$^2D^o$–$2s^22p^2(^1D)10d(^2D)$
	...	−0.008	...	34.311	$^2D^o$–$2s^22p^2(^1D)10d(^2P)$
31	33.860	−0.020	(0.0045)	34.311	$^2D^o$–$2s^22p^2(^1D)11d(^2F)$
	...	−0.020	...	34.311	$^2D^o$–$2s^22p^2(^1D)11d(^2D)$
	...	−0.020	...	34.311	$^2D^o$–$2s^22p^2(^1D)11d(^2P)$
32	33.910	0.071	0.0061	35.458	$^2P^o$–$2s^22p^2(^1S)6d(^2D)$
33	33.933	−0.045	(0.0032)	34.311	$^2D^o$–$2s^22p^2(^1D)12d(^2F)$
	...	−0.045	...	34.311	$^2D^o$–$2s^22p^2(^1D)12d(^2D)$
	...	−0.045	...	34.311	$^2D^o$–$2s^22p^2(^1D)12d(^2P)$
34	33.991	−0.100	(0.0025)	34.311	$^2D^o$–$2s^22p^2(^1D)13d(^2F)$
	...	−0.100	...	34.311	$^2D^o$–$2s^22p^2(^1D)13d(^2D)$
	...	−0.100	...	34.311	$^2D^o$–$2s^22p^2(^1D)13d(^2P)$
35	34.036	−0.142	(0.0021)	34.311	$^2D^o$–$2s^22p^2(^1D)14d(^2F)$
	...	−0.142	...	34.311	$^2D^o$–$2s^22p^2(^1D)14d(^2D)$
	...	−0.142	...	34.311	$^2D^o$–$2s^22p^2(^1D)14d(^2P)$
36	34.072	−0.181	(0.0015)	34.311	$^2D^o$–$2s^22p^2(^1D)15d(^2F)$
	...	−0.181	...	34.311	$^2D^o$–$2s^22p^2(^1D)15d(^2D)$
	...	−0.181	...	34.311	$^2D^o$–$2s^22p^2(^1D)15d(^2P)$
37	34.102	−0.249	(0.0009)	34.311	$^2D^o$–$2s^22p^2(^1D)16d(^2F)$
	...	−0.249	...	34.311	$^2D^o$–$2s^22p^2(^1D)16d(^2D)$
	...	−0.249	...	34.311	$^2D^o$–$2s^22p^2(^1D)16d(^2P)$

TABLE 4—*Continued*

Feature	Energy (eV)	Quantum Defect δ	Oscillator Strength[a]	Series Limit (eV)	Assignment
38	34.127	−0.334	(0.0004)	34.311	$^2D^o$–$2s^22p^2(^1D)17d(^2F)$
	...	−0.334	...	34.311	$^2D^o$–$2s^22p^2(^1D)17d(^2D)$
	...	−0.334	...	34.311	$^2D^o$–$2s^22p^2(^1D)17d(^2P)$
39	34.328	0.060	0.0050	35.458	$^2P^o$–$2s^22p^2(^1S)7d(^2D)$
40	34.597	0.050	0.0033	35.458	$^2P^o$–$2s^22p^2(^1S)8d(^2D)$
41	34.782	0.028	0.0027	35.458	$^2P^o$–$2s^22p^2(^1S)9d(^2D)$
42	34.909	0.044	0.0010	35.458	$^2P^o$–$2s^22p^2(^1S)10d(^2D)$
43	35.008	0.004	0.0015	35.458	$^2P^o$–$2s^22p^2(^1S)11d(^2D)$
44	35.082	−0.030	0.0014	35.458	$^2P^o$–$2s^22p^2(^1S)12d(^2D)$
45	35.121	...	...	...	$^4S^o$ threshold
46	35.145	−0.185	0.0018	35.458	$^2P^o$–$2s^22p^2(^1S)13d(^2D)$
47	35.183	−0.066	0.0005	35.458	$^2P^o$–$2s^22p^2(^1S)14d(^2D)$
48	35.219	−0.088	0.0008	35.458	$^2P^o$–$2s^22p^2(^1S)15d(^2D)$
49	37.604	0.551	0.0370	46.707	$^2D^o$–$2s2p^3(^3D^o)3p(^2P)$
50	38.216	0.477	0.0457	42.586	$^4S^o$–$2s2p^3(^5S^o)4p(^4P)$
51	38.376	...	...	...	Unassigned
52	38.686	0.391	0.0026	46.620	$^2D^o$–$2s2p^3(^3D^o)3p(^2F)$
53	38.940	...	...	...	Unassigned
54	39.478	0.436	0.0012	47.527	$^2P^o$–$2s2p^3(^3P^o)3p(^2D)$ (?)
55	39.919	0.495	0.0217	42.586	$^4S^o$–$2s2p^3(^5S^o)5p(^4P)$
56	40.773	0.543	0.0080	42.586	$^4S^o$–$2s2p^3(^5S^o)6p(^4P)$
57	41.206	0.753	0.0024	42.586	$^4S^o$–$2s2p^3(^5S^o)7p(^4P)$
58	41.674	0.336	0.0035	42.586	$^4S^o$–$2s2p^3(^5S^o)8p(^4P)$
59	41.878	0.321	0.0023	42.586	$^4S^o$–$2s2p^3(^5S^o)9p(^4P)$
60	42.021	0.309	0.0009	42.586	$^4S^o$–$2s2p^3(^5S^o)10p(^4P)$
61	42.121	0.346	0.0053	42.586	$^4S^o$–$2s2p^3(^5S^o)11p(^4P)$
62	42.149	0.534	0.0027	46.707	$^2D^o$–$2s2p^3(^3D^o)4p(^2P)$
63	42.167	0.795	0.0073	42.586	$^4S^o$–$2s2p^3(^5S^o)12p(^4P)$
64	42.409	0.430	0.0032	46.620	$^2D^o$–$2s2p^3(^3D^o)4p(^2F)$
65	42.547	...	...	...	Unassigned
66	43.115	0.576	0.0026	47.527	$^2P^o$–$2s2p^3(^3P^o)4p(^2D)$ (?)
67	43.285	...	...	...	Unassigned
68	43.946	...	...	...	Unassigned
69	43.977	0.511	0.0033	46.707	$^2D^o$–$2s2p^3(^3D^o)5p(^2P)$
70	44.072	0.430	0.0017	46.620	$^2D^o$–$2s2p^3(^3D^o)5p(^2F)$
71	44.882	0.496	0.0016	46.707	$^2D^o$–$2s2p^3(^3D^o)6p(^2P)$
72	44.919	0.438	0.0012	46.620	$^2D^o$–$2s2p^3(^3D^o)6p(^2F)$
73	45.093	0.480	0.0031	47.527	$^2P^o$–$2s2p^3(^3P^o)5p(^2D)$ (?)
74	45.402	0.470	0.0025	46.707	$^2D^o$–$2s2p^3(^3D^o)7p(^2P)$
75	45.658	0.696	0.0008	46.707	$^2D^o$–$2s2p^3(^3D^o)8p(^2P)$
76	45.943	0.397	0.0009	46.707	$^2D^o$–$2s2p^3(^3D^o)9p(^2P)$

NOTES.—Square brackets indicate that the assignment of the oscillator strength is uncertain because different components in the primary beam contribute to the observed feature. Parentheses indicate that multiple features from the same initial state might be present. "(?)" indicates that the assignments of these features are questionable.

[a] Measured oscillator strengths have been multiplied by 6.66, 2.38, or 2.33 depending on the assigned initial state, since the population fractions of the ion beam of $^2P^o$, $^2D^o$, or $^4S^o$ were 0.15, 0.42, and 0.43, respectively. A unit branching ratio for autoionization has been assumed.

[b] In this feature the assignment of the oscillator strength is uncertain because of the presence of structure from the $^2D^o$ and $^2P^o$. However, it has been multiplied by 2.38 because clearly the dominant structure is from the $^2D^o$ metastable fraction of the beam.

[c] These features were measured at a resolution of 5 meV in order to resolve them.

Finally, in Figures 8, 9, and 10, the experimental data are compared with two independent *R*-matrix calculations (A and B), which differ primarily in the number of basis terms used, and with the TOPbase data. Calculations A and B have been shifted slightly in energy to match the known threshold energies. To facilitate comparison with the experiment, the theoretical cross sections for photoionization from the ground and metastable states have been multiplied by their estimated experimental fractions and summed. A Gaussian with 17 meV FWHM has also been convoluted with the calculations to represent the instrumental resolution. All three calculations agree within 25% on the direct photoionization cross section, and with the absolute measurements within 40%. The predicted resonance structure differs considerably between the three close-coupling *R*-matrix calculations, the TOPbase data being the least accurate in the prediction of resonance positions and intensities. The satisfactory agreement between experiment and theory for the nonresonant cross section in the threshold energy region substantiates the ground-state fraction determined by the beam-attenuation method.

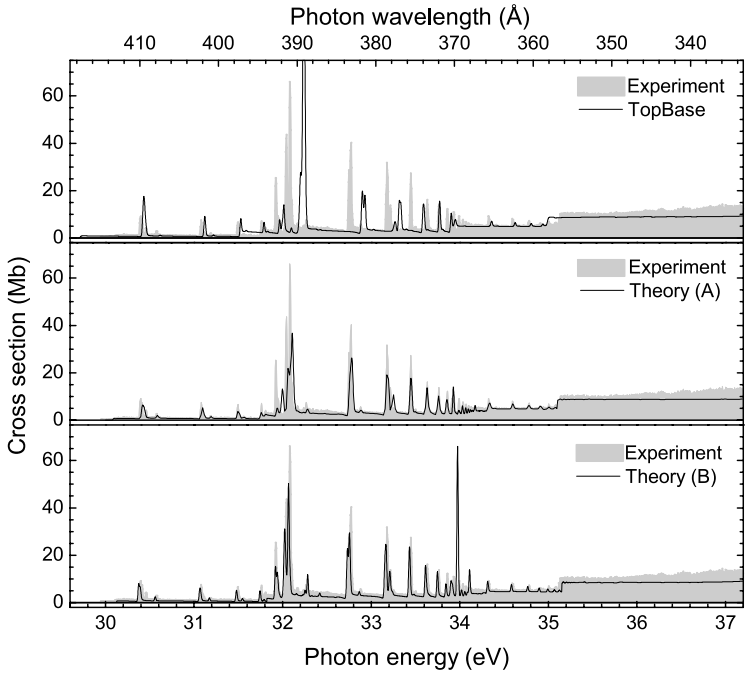

FIG. 8.—Comparison of absolute cross section photoionization measurements from 30.0 to 37.2 eV with the TOPbase and two independent *R*-matrix calculations. All calculations have been convoluted with a 17 meV FWHM Gaussian distribution, and their relative energy scales have been adjusted, except for the TOPbase calculation, to the standard reference values for the $^2P^o$, $^2D^o$, and $^4S^o$ ionization thresholds. The theoretical cross sections for each initial state have been multiplied by the experimental fractions (0.15, 0.42, and 0.43, respectively) and summed.

5. SUMMARY

The effective absolute photoionization cross section from a mixture of ground state and metastable states of O^+ has been presented from 29.9 to 46.0 eV (414.7 to 269.5 Å) with an energy resolution of 17 meV. Seventy-six features were resolved in the measurements. Most of these have been assigned spectroscopically and characterized in terms of energy, quantum defect, and oscillator strength. The absolute measurements are in agreement within 40% with two independent *R*-matrix calculations and with the TOPBase data. The agreement with respect to the resonance features

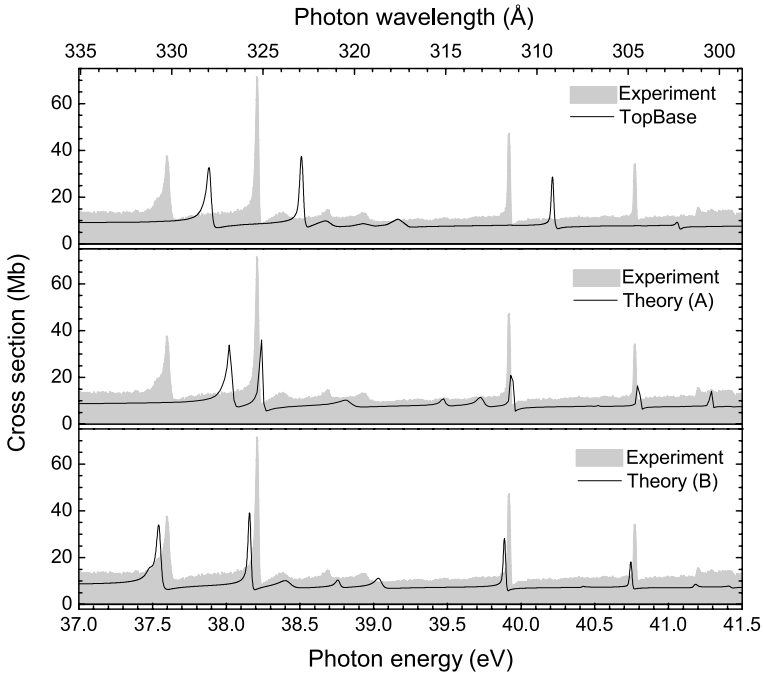

FIG. 9.—Comparison of absolute photoionization cross section measurements from 37.0 to 41.5 eV with the TOPbase and two independent *R*-matrix calculations.

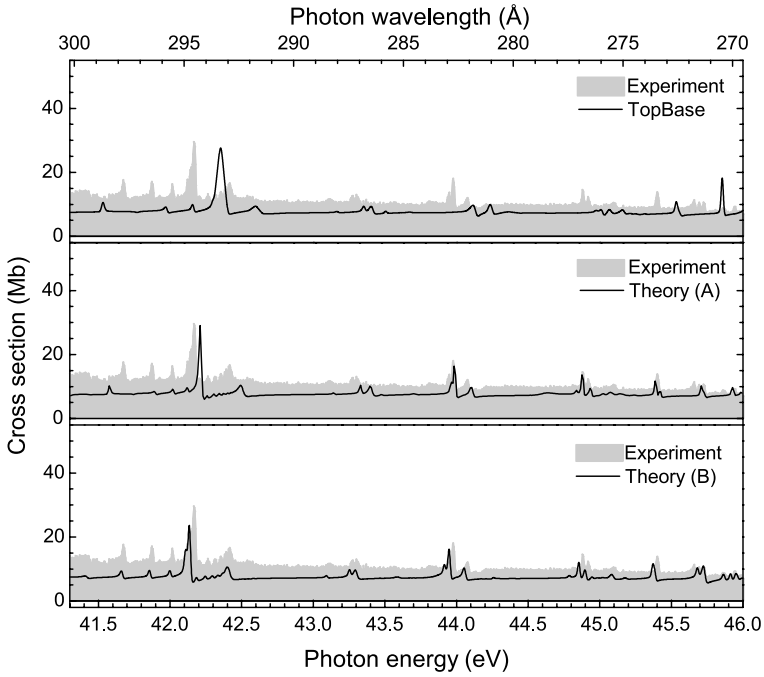

FIG. 10.—Comparison of absolute photoionization cross section measurements from 41.3 to 46.0 eV with the TOPbase and two independent *R*-matrix calculations.

is better with the two new calculations than with the TOPBase data. These data constitute the first of a series of measurements along the isoelectronic sequence of nitrogen.

This collaborative research was supported in part by the DOE Division of Chemical Sciences, Geosciences, and Biosciences from grant DE-FG03-97ER14787, by the DOE Facilities Initiative, by Nevada DOE/EPSCoR and by CONACyT. A. Aguilar acknowledges a fellowship granted by DGAPA-UNAM Mexico. M. M. Sant'Anna acknowledges the CNPq-Brazil for a postdoctoral fellowship at the ALS. S. Nahar acknowledges partial support from NSF grant AST-9870089. Part of the computational work was carried out on the Cray YMP at the Ohio Supercomputer Center. B. McLaughlin acknowledges support from ITAMP, which is funded by a grant to Smithsonian Astrophysical Observatory and Harvard University. Excellent technical support was provided by W. Brinsmead, W. Cline, D. Meredith, and W. Weaver of the University of Nevada, Reno, in the fabrication of the end station, and by B. Rude of the Advanced Light Source.

REFERENCES

Aggarwal, K. M., & Hibbert, A. 1991a, J. Phys. B, 24, 3445
———. 1991b, J. Phys. B, 24, 4685
Burke, P. G., & Berrington, K. A. 1993, Atomic and Molecular Processes: an *R*-matrix Approach (Bristol: Inst. Phys.)
Carr, S. S., Niciejewski, R. J., & Killeen, T. L. 1993, Geophys. Res. Lett., 20, 2035
Covington, A. M., et al. 2001, Phys. Rev. Lett., 87, 243002
———. 2002, Phys. Rev. A, 66, 062710
Cunto, W., Mendoza, C., Ochsenbein, F., & Zeippen, C. J. 1993, A&A, 275, L5 (TOPbase)
Hummer, D. G., Berrington, K. A., Eissner, W., Pradhan, A. K., Saraph, H. E., & Tully, J. A. 1993, A&A, 279, 298
Iglesias, C. A., & Rogers, F. J. 1996, ApJ, 464, 943
Kjeldsen, H., Andersen, P., Folkmann, F., Knudsen, H., Kristensen, B., West, J. B., & Andersen, T. 2000a, Phys. Rev. A, 62, 20702
Kjeldsen, H., Kristensen, B., Folkmann, F., & Andersen, T. 2002a, J. Phys. B, 35, 3655
Kjeldsen, H., Folkmann, F., Knudsen, H., Rasmussen, M. S., West, J. B., & Andersen, T. 1999a, J. Phys. B, 32, 4457
———. 1999b, ApJ, 524, L143
Kjeldsen, H., Hansen, J. F., Folkmann, F., Knudsen, H., West, J. B., & Andersen, T. 2001, ApJS, 135, 285
Kjeldsen, H., Kristensen, B., Brooks, R. L., Folkmann, F., Knudsen, H., & Andersen, T. 2002b, ApJS, 138, 219
Kjeldsen, H., West, J. B., Folkmann, F., Knudsen, H., & Andersen, T. 2000b, J. Phys. B, 33, 1403
Kristensen, B., Andersen, T., Folkman, F., Kjeldsen, H., & West, J. B. 2002, Phys. Rev. A, 65, 22707
Le Dourneuf, M., Vo Ky Lan, & Zeippen, C. J. 1979, J. Phys. B, 12, 2449
Lindsay, B. G., Merrill, R. L., Straub, H. C., Smith, K. A., & Stebbings, R. F. 1998, Phys. Rev. A, 57, 331
Lyon, I. C., Peart, B., & Dolder, K. 1987a, J. Phys. B, 20, 1925
Lyon, I. C., Peart, B., Dolder, K., & West, J. B. 1987b, J. Phys. B, 20, 1471
Lyon, I. C., Peart, B., West, J. B., & Dolder, K. 1986, J. Phys. B, 19, 4137
Lyon, I. C., Peart, B., West, J. B., Kington, A. E., & Dolder, K. 1984, J. Phys. B, 17, L344
Meier, R. R. 1991, Space Sci. Rev., 58, 1
Melendez-Alvira, D. J., Meier, R. R., Picone, J. M., Feldman, P. D., & McLaughlin, B. M. 1999, J. Geophys. Res., 104, 14901
Müller, A., et al. 2002, J. Phys. B, 35, L137
Nahar, S. N. 1998, Phys. Rev. A, 58, 3766
Peart, B., & Lyon, I. C. 1987, J. Phys. B, 20, L673
Peart, B., Lyon, I. C., & Dolder, K. 1987, J. Phys. B, 20, 5403
Rogers, F. J., & Iglesias, C. A. 1992, ApJS, 79, 507
Seaton, M. J. 1987, J. Phys. B, 20, 6363
Schippers, S., et al. 2002, Phys. Rev. Lett., 89, 193002
West, J. B. 2001, J. Phys. B, 34, R45
Wiese, W. L., Fuhr, J. R., & Deters, T. M. 1996, J. Phys. Chem. Ref. Data Monograph 7